How to cite: *Angew. Chem. Int. Ed.* **2023**, *62*, e202312314
doi.org/10.1002/anie.202312314

Nanographenes

Tetrahedraphene: A Csp^3-centered 3D Molecular Nanographene Showing Aggregation-Induced Emission

Arturo Oró, Fernando Romeo-Gella, Josefina Perles, Jesús M. Fernández-García, Inés Corral,* and Nazario Martín**

Dedicated to Professor Maurizio Prato on the occasion of his 70th birthday

Abstract: The bottom-up synthesis of 3D tetrakis(hexa-peri-hexabenzocoronenyl)methane, "tetrahedraphene", is reported. This molecular nanographene constituted by four hexa-*peri*-hexabenzocoronene (HBC) units attached to a central sp^3 carbon atom, shows a highly symmetric arrangement of the HBC units disposed in the apex of a tetrahedron. The X-ray crystal structure reveals a tetrahedral symmetry of the molecule and the packing in the crystal is achieved mostly by CH···π interactions since the interstitial solvent molecules prevent the π···π interactions. In solution, tetrahedraphene shows the same electrochemical and photophysical properties as the hexa-^{t}Bu-substituted HBC (^{t}Bu-HBC) molecule. However, upon water addition, it undergoes a fluorescence change in solution and in the precipitated solid, showing an aggregation induced emission (AIE) process, probably derived from the restriction in the rotation and/or vibration of the HBCs. Time-Dependent Density Functional Theory (TDDFT) calculations reveal that upon aggregation, the high energy region of the emission band decreases in intensity, whereas the intensity of the red edge emission signal increases and presents a smoother decay, compared to the non-aggregated molecule. All in all, the excellent correlation between our simulations and the experimental findings allows explaining the colour change observed in the different solutions upon increasing the water fraction.

Introduction

The invention of transistors 75 years ago resulted in the electronic revolution experienced since the second half of the 20th century. In 1965, Moore predicted that the number of transistors on an integrated circuit would double every two years. Moore's law became true and today the number of transistors used on a microchip is of the order of billions, making necessary a nanometer-scale miniaturization of the semiconductor systems. In the last decade, nanographenes (NGs), fragments of graphene in which the electrons are confined in a nano-sized structure making it possible the opening of a gap between the valence and the conduction bands,[1] have been employed as semiconductors in the construction of field effect transistors (FET),[2] but also in other electronic applications; namely, energy storage,[3] bioimaging,[4] OLEDs[5] or photovoltaics.[6]

NGs have usually been synthesized following a top-down approach by "cutting" a graphene sheet into smaller fragments using chemical or physical methods.[7] Although this methodology starts from readily accessible bulk materials and it is easily scalable, it does not allow a fine control of the properties due to the polydispersion in sizes and shapes of the final material. In contrast, the bottom-up approach in which NGs are grown up from smaller chemical entities using solution-phase benchtop organic synthesis,[8] leads to monodisperse molecules with a precise control on the size and shape, exhibiting fine-tuned optoelectronic properties.

[*] A. Oró, Dr. J. M. Fernández-García, Prof. Dr. N. Martín
Departamento de Química Orgánica, Facultad de Química, Universidad Complutense de Madrid
Avd. Complutense S/N, 28040 Madrid (Spain)
E-mail: jesusmaf@ucm.es
nazmar@ucm.es

F. Romeo-Gella, Prof. Dr. I. Corral
Departamento de Química, Facultad de Ciencias, Universidad Autónoma de Madrid
28049 Madrid (Spain)
E-mail: ines.corral@uam.es

Dr. J. Perles
Laboratorio de Difracción de Rayos X de Monocristal, SIdI, Universidad Autónoma de Madrid
C/Francisco Tomás y Valiente, 7. Campus de Cantoblanco, 28049 Madrid (Spain)

Prof. Dr. I. Corral
Institute for Advanced Research in Chemical Sciences (IAdChem), Universidad Autónoma de Madrid
28049 Madrid (Spain)

Prof. Dr. N. Martín
IMDEA-Nanociencia
C/Faraday, 9. Campus de Cantoblanco, 28049 Madrid (Spain)

Thus, taking advantage of the versatility that provides the set of organic reactions available, and the selectivity of these transformations depending on the reaction conditions,[9] a large number of molecular NGs have been synthetized by design in the recent years.[10] An example of this control is the introduction of out-of-plane defects at will, namely curvature,[11] helicity,[12] or strain,[13] resulting in the presence of chirality as an additional and remarkable structural control.[14]

Hexa-*peri*-hexabenzocoronene (HBC) is considered the simplest molecular nanographene and, due to its easy preparation and good stability, many of the synthesized molecular nanographenes are based on this molecular fragment (Figure 1). It is worth noting that *tert*-butyl groups are usually required for improving solubility and facilitate the chemical and crystallographic characterization.[15] In this regard, Lucas and co-workers described the preparation of triarylphosphines bearing one to three penta-*tert*-butyl substituted HBC units. These "superphenylphosphines" maintain the properties of HBC, including strong optical absorption, blue emission and redox activity. Additionally, they can act as ligands to form Pd complexes, which display catalytic activity similar to that of other commonly used Pd complexes.[16] Furthermore, the stoichiometry and the isomerism in the formation of these complexes strongly depends on the number of HBCs in the phosphines. Another singular example reported by Wu and Wang consists in NGs based on three HBCs, endowed with one *tert*-butyl group each, attached to a central nitrogen atom.[17] Taking advantage of the HBC′s high capacity for lithium incorporation and its tendency to form aggregates by π–π stacking,[18] they used these materials as anode electrodes for high-performance lithium-ion batteries.

Another consequence observed in molecules with high tendency for aggregation endowed with mobile parts, is the different photophysical behavior in the solution phase with respect to the solid phase. Normally, aggregation-induced changes in fluorescence are the result of the restriction of the rotation and the vibration of parts of the molecules that in the solution phase contribute to non-radiative relaxation processes.[19] Thus, many examples of aggregation-induced emission (AIE) or aggregation-induced emission enhancement (AIEE) have been described since the early 2000s.[20] Recently, molecules exhibiting AIE have received a lot of attention due to their interest for the fabrication of OLEDs, provided that these devices operate as thin films and crystals.[21]

Herein, we describe the facile synthesis of a singular molecular nanographene based on four penta-*tert*-butyl-HBC moieties attached to a central sp^3 carbon atom. Single crystal X-ray diffraction confirms the tetrahedral arrangement of the molecule and a packing in the crystal by CH···π interactions. Interestingly, the photophysical study of **1** reveals that, upon water addition, this system experiences a bathochromic shift in the emission both in solution and in the precipitated solid. TDDFT calculations nicely underpin that this aggregation-induced emission could be derived from the high predisposition of HBCs to stack by π–π interactions, which restricts the rotation and/or vibration of these fragments. It is worth mentioning that, in contrast to previous NGs endowed with topological defects obtained in the search for AIE,[22] the tetrahedral arrangement of the planar HBC units in molecule **1** allows the intermolecular π–π overlapping, thus leading to the observed experimental findings.

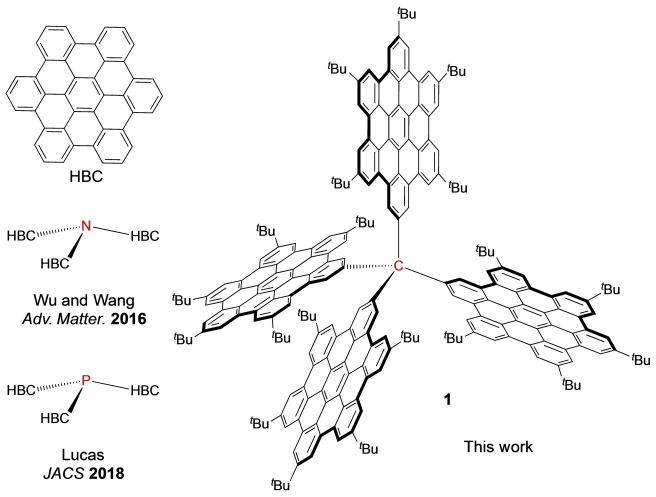

Figure 1. Pristine HBC and HBC-based molecular nanographenes containing a central sp^3 atom.

Results and Discussion

The most classical bottom-up methodology used in the preparation of molecular NGs, starts with the π-extension of an aromatic central scaffold that leads to polyphenylenic structures.[23] Then, a graphitization process, usually employing the Scholl oxidation reaction,[10a] generates the hexagonal lattice featured by graphenic derivatives.

For the synthesis of tetrakis(penta-*tert*-butyl-hexa-peri-hexabenzocoronenyl)methane **1**, we proposed a single sp^3-hybridized carbon atom as the central scaffold in order to obtain a molecular nanographene consisting of four HBCs arranged in a tetrahedral disposition.

Thus, tetrahedraphene **1** has been readily prepared in three synthetic steps starting from commercially available tetrakis(4-bromophenyl)methane **2** (Scheme 1).

The first two steps aimed for the π-extension of compound **2**. Firstly, a four-fold Pd-catalysed Sonogashira cross-coupling reaction afforded the tetrakisalkynylmethane **3** in a very good yield (88 %). Compound **3** shows, as expected, a small signal in the FTIR spectrum at 2215 cm^{-1} corresponding to the presence of the alkyne group (Figure S4, see Supporting Information). Thereafter, a four-fold [4+2] cycloaddition reaction between **3** and cyclopentadienone **4**, followed by in situ chelotropic CO extrusion, led to polyphenylene **5** (89 %). It should be noted the high performance of the π-extension of the central scaffold, having a 78 % overall yield in two quadruple synthetic steps. The last step of the synthesis consisted in a cyclodehydrogenative C–C coupling by Scholl oxidation using 2,3-dichloro-

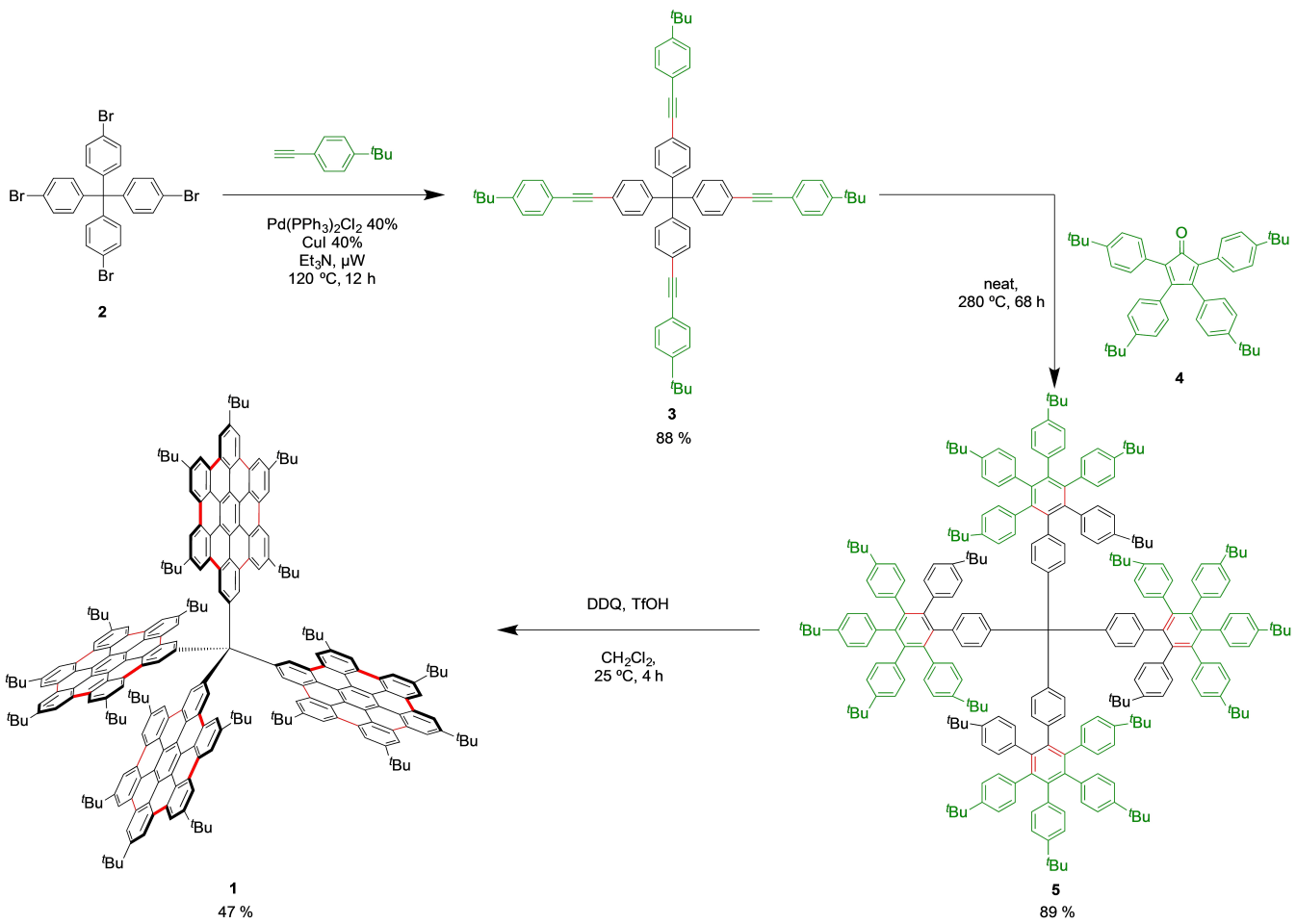

Scheme 1. Synthetic pathway towards tetrahedraphene **1** starting from tetrakis(4-bromophenyl)methane **2**. The synthesis consists in three steps: 1) Sonogashira cross-coupling reaction, 2) Diels–Alder cycloaddition reaction and 3) Scholl oxidation. Each reaction step results in the formation of new C–C bonds (highlighted in red) and new fragments incorporated (marked in green).

5,6-dicyano-*p*-benzoquinone (DDQ) as the oxidant. In this reaction, the graphitization of the polyphenylene **5** by formation of 24 new C–C bonds afforded the final tetrahedral molecular nanographene **1**.

Tetrahedraphene **1** was characterized by high resolution mass spectrometry (calculated for $C_{249}H_{228}$ = 3217.7841, found = 3217.7746), and by FT-IR and NMR spectroscopies. ^{1}H NMR spectrum shows only three signals in the aliphatic region with relative intensities 2:2:1, and five signals (one of them with double intensity) in the aromatic region. These signals correspond with the three *tert*-butyl groups and the six aromatic hydrogens of a half HBC, respectively, thus revealing the tetrahedral symmetry of the molecule.

The crystal structure of **1** (Figure 2) was solved by single crystal X-ray diffraction from a cocrystal containing interstitial THF, *n*-hexane and methanol molecules for an overall formula **1**·C_4H_8O·CH_3OH·0.25 C_6H_{12} (Section 6, see Supporting Information).[24] Compound **1** is highly symmetrical: its central carbon atom (C63) is located at an inversion center from a fourfold rotoinversion axis, with only a quarter of the molecule present in the asymmetric unit (Figure S28, see Supporting Information). The HBC moiety is nearly planar, with a maximum deviation of 0.272 Å for peripheral C10 (Figure S30, see Supporting Information), although the larger probability ellipsoids for some exterior carbon atoms prove the flexibility of these layers (Figure S28 right of the Supporting Information). This bendability of the HBC fragments allows them to optimize supramolecular interactions and has previously been observed in other molecules reported by our group containing this moiety.[9b][12e][12g] The packing of **1** in the crystal is heavily influenced by the existence of interstitial solvent molecules, as the THF located between the four blades of the same molecule (Figure S31, see Supporting Information) and the *n*-hexane between molecules of **1** (Figure 2b). These interactions prevent any π···π stacking similar to the one found in the crystal structures of the "superphenylphosphines" reported by Lucas et al.[16] The role of the solvents and their C–H···π supramolecular interactions have proved crucial in the physical properties displayed by this compound, as described below.

The electrochemical properties of compound **1** were explored by cyclic voltammetry and Differential Pulse Voltammetry (DPV) in toluene/acetonitrile 4:1 with a

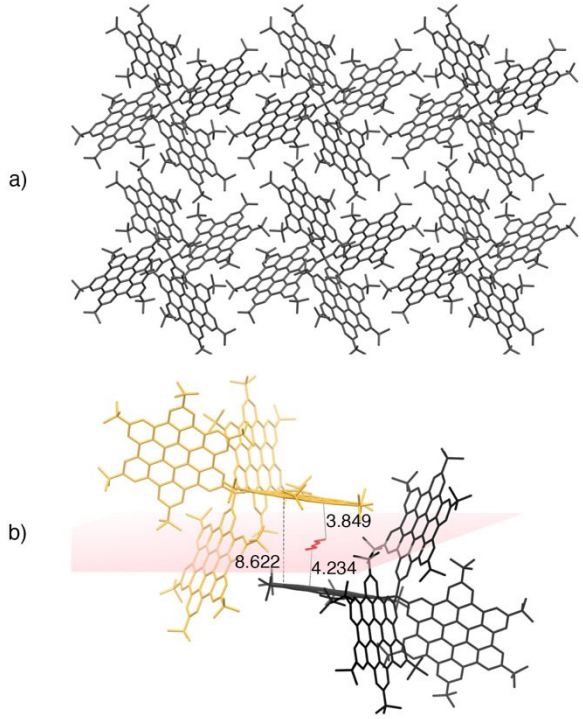

Figure 2. a) View along the crystallographic *c* axis of the square packing of the tetrahedraphene molecules c) Detail of the *n*-hexane (in red) molecule trapped between two aromatic layers of neighbor molecules of **1** (in orange and black); distances (Å) from the plane of the solvent molecule to the two neighbor π systems (right) and closest distance between carbon atoms in adjacent HBC layers (left, atoms C4-C19).

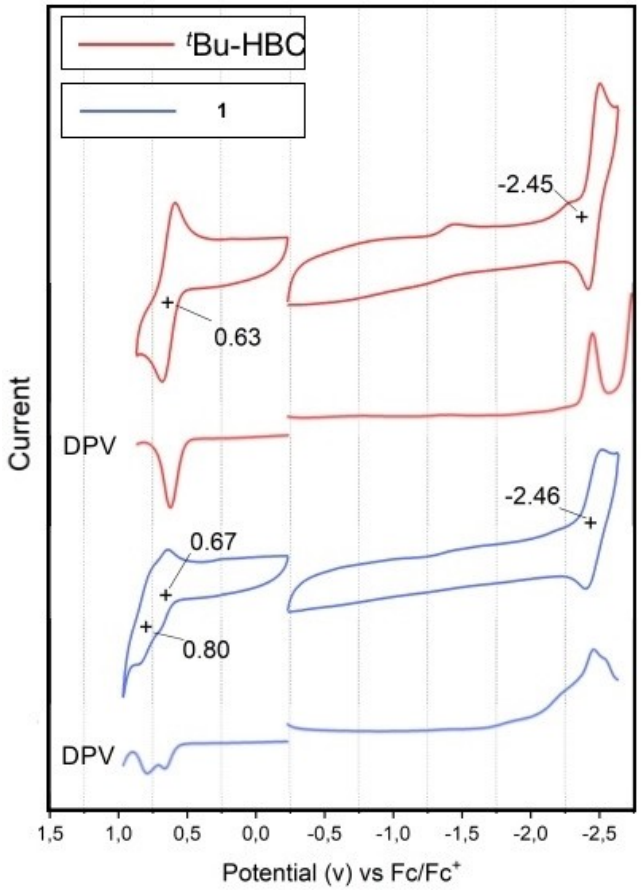

Figure 3. First reduction and oxidation potentials and Differential Pulse Voltammetry (DPV) of ^{t}Bu-HBC (red) and **1** (blue) in toluene: acetonitrile 4:1 with tetrabutylammonium hexafluorophosphate 0.1 M solution as the supporting electrolyte at room temperature. Glassy carbon was used as the working electrode, $Ag/AgNO_3$ as the reference electrode and platinum as the counter electrode. All redox potentials are referenced to Fc/Fc^+.

tetrabutylammonium hexafluorophosphate 0.1 M solution as the supporting electrolyte and the results obtained were referred to Fc/Fc^+. First reduction and oxidation potentials were compared with those of the hexa-^{t}Bu-substituted HBC (^{t}Bu-HBC, Figure 3). On the one hand, when applying negative potentials, a cathodic wave appeared at −2.51 V with the corresponding quasi reversible anodic wave at −2.39 V (Figure S22 see Supporting Information), giving a half-wave first reduction potential value of $E^1_{1/2\ red} = -2.46$ V. Compared with that of ^{t}Bu-HBC (−2.45 V), both compounds have the same very poor electron acceptor character. Additionally, at more negative voltages, a second and a third irreversible waves appear with cathodic potentials of $E^2_{red} = -2.98$ V and $E^3_{red} = -3.11$ V (Figure S23, see Supporting Information). On the other hand, at positive potentials, tetrahedraphene **1** shows two anodic waves at 0.70 and 0.85 V (Figure S22 see Supporting Information). These peaks present two quasi reversible cathodic waves at 0.62 and 0.74 V, respectively, giving rise to two half-wave oxidation potentials of $E^1_{1/2\ ox} = 0.67$ V and $E^2_{1/2\ ox} = 0.80$ V, respectively (Figure 3). Compared to the oxidation voltammogram of ^{t}Bu-HBC, which presents a unique oxidation potential at $E^1_{1/2\ ox} = 0.63$ V, compound **1** shows that the formation of the radical-cation in **1** shifts the release of a second electron to slightly more positive values as expected, due to a repulsive interaction between the two generated positive charges in the dication.

The HOMO–LUMO gap of **1** (calculated HOMO and LUMO can be found in Figure S33, see Supporting Information) was experimentally determined by the onset potentials of the first oxidation and reduction waves using DPV (Figure S25, see Supporting Information), showing a value of 2.85 eV. This value is in line with the computationally predicted HOMO–LUMO gap of 3.49 eV. Compared to that of ^{t}Bu-HBC (2.82 eV, Figure S26, see Supporting Information), the band gap is very similar, as expected by the lack of conjugation between the four HBC units in **1**.

Absorption and fluorescence properties of the molecular NG **1** were explored and compared with that of ^{t}Bu-HBC. The absorption and emission spectra of **1** and ^{t}Bu-HBC in $CHCl_3$ are shown in Figure 4. At first sight, both molecules show a similar photophysical behavior. The absorption spectrum of tetrahedraphene **1** shows a main band in the UV region at 365 nm, with a shoulder at 349 nm, and an additional sharp band at 395 nm (Table 1). Compared to the spectrum of ^{t}Bu-HBC (344, 360 and 390), the bands of **1** are slightly red-shifted (5 nm) and broadened. It is worth noting

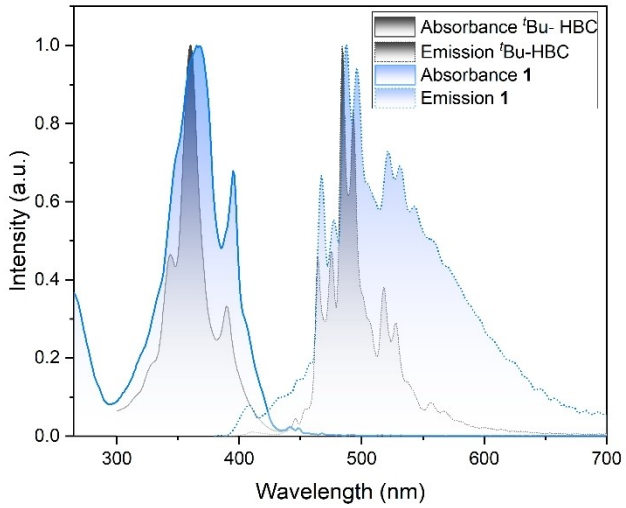

Figure 4. Absorption and emission spectra of ^{t}Bu-HBC (grey) and **1** (blue) in $CHCl_3$. Emission spectra were recorded with an excitation wavelength of 365 nm.

that the extinction coefficient values for **1** are significantly larger than those observed for ^{t}Bu-HBC (Table 1).

The broad shape of the absorption spectrum of **1** can be explained by the existence of more rotational and vibrational states, derived from the relative motions of the four units of HBC.

In the visible region both molecules show forbidden transition bands with low molar extinction coefficients. Once again, the bands of **1** (441 and 448 nm) appear red-shifted and broadened compared to those of ^{t}Bu-HBC (439, 441 and 445 nm).

The emission spectra of tetrahedraphene **1** and ^{t}Bu-HBC (Figure 4) show a similar fine structure and peaks from 464 to 567 nm with the bands of **1** slightly red-shifted. Whereas ^{t}Bu-HBC shows a weak red tail from 550 nm leading to blue-green emission, in **1** the red tail is much more intense, resulting in a purer green emission.

To discard a solvatochromic origin of this emission band, we performed fluorescence experiments in solvents with different polarities (Figure S18, see Supporting Information). In all the solvents where **1** was totally soluble, independently of their dielectric constant, the emission spectra spanned the same wavelength range and showed a very similar structure to that of ^{t}Bu-HBC, generating the same blue-green emission. Hence, a solvatochromic effect behind the appearance of the broad red tail was discarded.

Furthermore, tetrahedraphene **1** has an intense yellow emission in the solid state (Figure 5d). To shed light on this different fluorescence behavior in solution and in the solid state, we prepared a solution of **1**, 4.97 10^{-7} M in THF (good solvent), and various solutions with different volume fractions of water (bad solvent), maintaining the concentration constant.

The emission spectra of these solutions show the blue-green emission of **1** (Figure 5a and Figure S19 of the Supporting Information) when employing water fractions of up to 0.45 vol % (Figures 5b and 5c). Within this range of water fractions, it can be observed a slight enhancement of the blue emission as the volume of water increases up to 0.3 vol % (see light blue spectrum in Figure 5a). However, when the water fraction reaches 0.5 vol %, two new broad bands can be observed at 543 and 582 nm (yellow spectrum in Figure 5a and Figure S20, see Supporting Information), which give rise to yellow emission (Figures 5b and 5c). When the water fraction is further increased, the intensity of the yellow emission decreases progressively (orange spectrum in Figure 5a).

Taking into account the molecular structure of tetrahedraphene **1**, the HBC groups have rotational and vibrational freedom in solution. As a poor solvent, namely water, is added, the HBC groups of different molecules start to undergo π–π interactions with the consequent formation of aggregates and the increase of the fluorescence quantum yield from 3.5 % in THF to 6.4 % with a volume water fraction of 0.9 (Figure S21, see Supporting Information). These values are, in turn, larger than those shown by ^{t}Bu-HBC (2.0 %), as the reference compound.[12g]

The aggregation restricts the rotation and vibration modes of the molecules and prevents the non-radiative relaxation of the excited state, leading to an enhancement of the blue-green emission up to 30 % water volume (AIEE process). A water fraction of 50 % produces a change in the color of the emission, which shifts the maximum to lower energies, in the range of yellow emission, as it is also observed in the solid state (AIE process). Surpassing 50 % of water fraction results in the precipitation of **1** and, consequently, the presence of less aggregates in suspension, leading to a decrease of the emission signal. This AIE process is the responsible for the intense red tail observed in Figure 4, as tetrahedraphene **1** is not completely soluble in $CHCl_3$.

To rationalize the origin of the change in the emission properties observed when augmenting the water fraction of the solvent, we have modelled the photophysical properties of the monomer and dimer of tetrahedraphene **1**. Our

Table 1: Absorption and emission spectra of ^{t}Bu-HBC and **1** in $CHCl_3$.

	Compound	$\lambda^{[a]}$ ($\varepsilon^{[b]}$)
Absorption	^{t}Bu-HBC	344 (63750), 360 (141700), 390 (46350), 439 (1600), 441 (1650), 445 (1800)
	Tetrahedraphene (**1**)	365 (396193), 395 (243478), 441 (9206), 448 (7729)
Emission	^{t}Bu-HBC	464, 475, 484, 493, 518, 528, 537, 556, 567
	Tetrahedraphene (**1**)	467, 477, 487, 496, 521, 531, 542

[a] nm. [b] $M^{-1}cm^{-1}$.

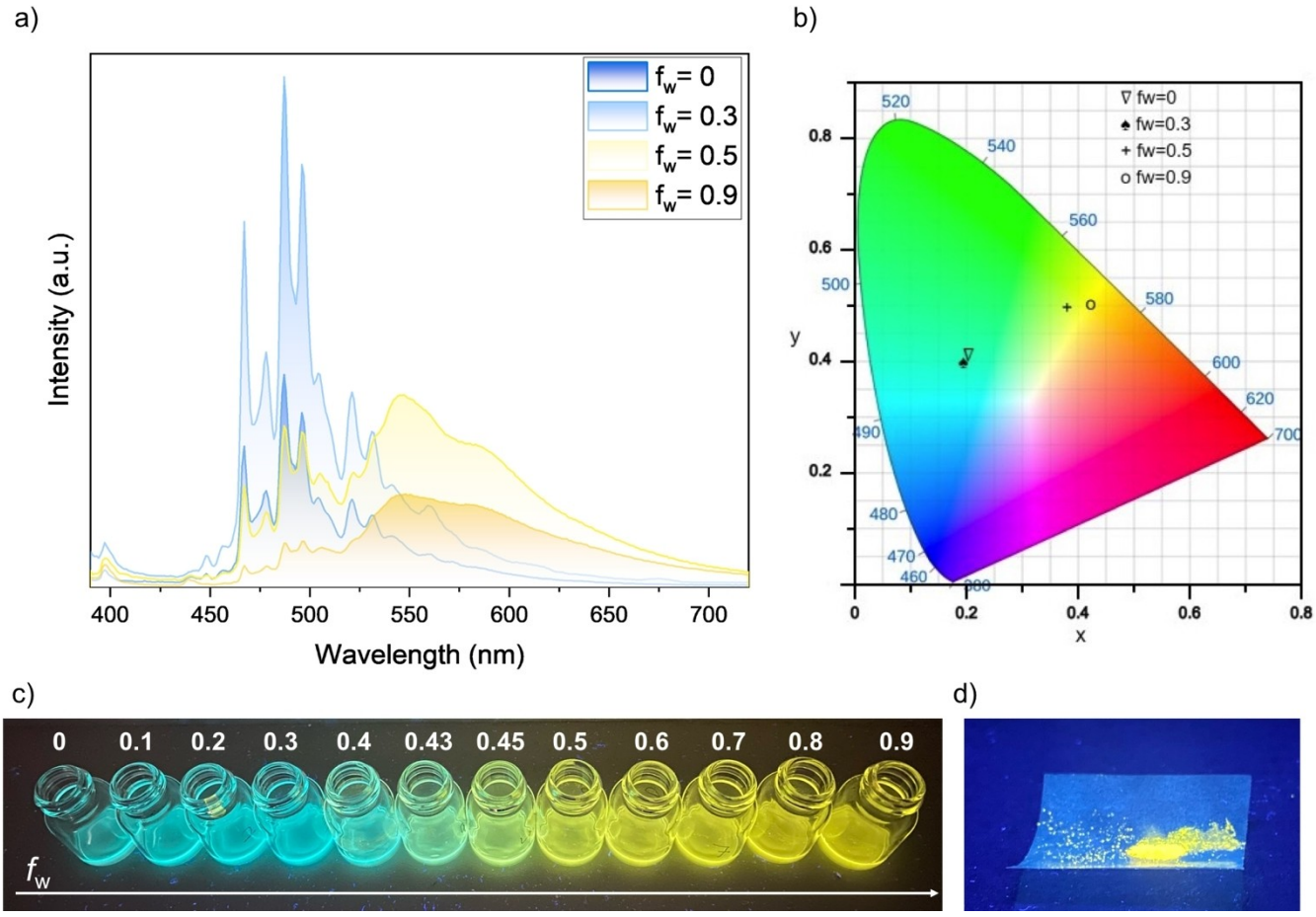

Figure 5. a) Emission spectra (excitation wavelength 365 nm) of **1**, 4.97 10^{-7} M in THF with different volume fractions of water (0, 0.3, 0.5 and 0.9). b) CIE chromaticity diagram 1931 of **1** in THF with different volume fractions of water (0, 0.3, 0.5 and 0.9). c) Emission of **1**, 4.97 10^{-7} M in THF with different volume fractions of water (f_w). d) Emission of **1** in the solid state.

simulations have been performed within the DFT framework and its linear response TDDFT version. In particular, we have resorted to the wB97X–D/def2-SV(P) protocol, to optimize the ground and first excited states of the monomer and dimer and to obtain the vertical excitation and emission energies. Since the ^{t}Bu groups are expected to play a negligible role in the photophysics of these systems, we have performed our simulations on a reduced model ignoring these substituents $\mathbf{1}_{red}$ (Figure S32, see Supporting Information). Importantly, this structural simplification does not seem to significantly affect the π–π interactions in the dimer, as supported by the similar distances calculated between the two interacting HBC moieties in the models including ($\mathbf{1}_{red,\ ^t\mathbf{Bu}}$ dimer) and lacking ($\mathbf{1}_{red}$ dimer) ^{t}Bu groups, which amount to 3.52 and 3.50 Å, respectively. The vertical excitation energies for the monomer and dimer are collected in Tables S2 and S3 (see Supporting Information). The natural transition orbitals involved in the lowest energy transitions of the monomer and the dimer are shown in Figures S35, S36 and S37 (see Supporting Information). Due to the symmetry of the system, the first four transitions in the monomer, each one delocalized along one or two of the HBC moieties, are dipole forbidden energetically degenerate excitations peaking at 3.52 eV, and correspond to the first excited state of isolated HBC. Coherently, S_5–S_8 and S_9–S_{12} group of transitions respectively peak at 3.75 and 4.27 eV and would correspond to the second and third excited state of the parent HBC. Systematically, the excitation energies in $\mathbf{1}_{red}$ are blue shifted by 0.1–0.2 eV compared to the parent HBC.[11g] For the dimer, the S_1 and S_2 states are also degenerate and localized on the π stacked HBC groups. Their vertical excitation energies are ca. 3.50 eV, coinciding with the energies of the monomer. Interestingly, the incorporation to the system of the ^{t}Bu groups, potentially interfering in the π–π staking, breaks the degeneracy of the first two states and produces a small red shift (0.1–0.2 eV) of the S_1 and S_2 excitation energies (see Supporting Information, Table S4). A vibrationally-resolved version of the absorption spectrum of the monomer can be found in the top panel of Figure 6, which shows an excellent agreement in terms of the spectral shape with the experimental results upon a red-shift of 0.7 eV. From the inspection of Figure 6, we conclude that the main absorption band of the spectrum arises from the higher-lying states, particularly S_{10}–S_{11}, while the lower energy and intensity region of the absorption spectra is ascribed to the lowest

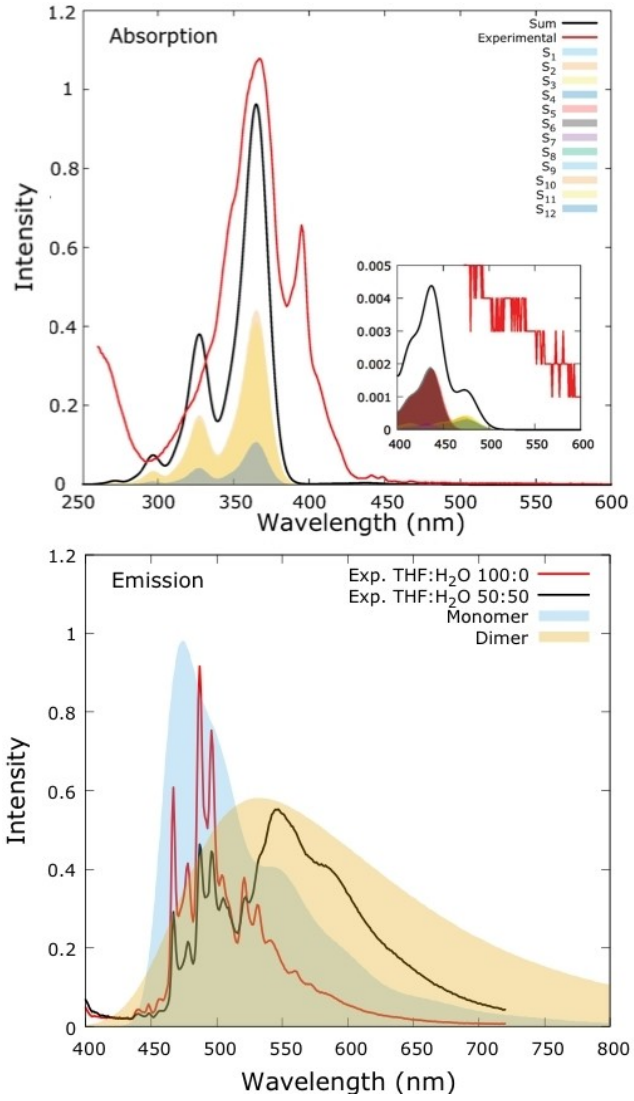

Figure 6. (Top) Vibrationally-resolved calculated absorption spectrum of $\mathbf{1}_{red}$ monomer, including the first ten excited states, (a red-shifted 0.7 eV has been applied). A zoom of the low energy region of the absorption spectrum has also been included. (Bottom) Vibrationally-resolved S_1 emission spectra of $\mathbf{1}_{red}$ monomer and dimer, (red shifts of 0.8 eV and 1.2 eV have been respectively applied).

lying and weakly absorbing states S_1–S_8 (Table S2 and Figure S34, see Supporting Information).

Aiming at interpreting the change of the emission spectra with the nature of the solvent, we undertook a search of the S_1 minima for the monomer and the dimer. The two minima very much resemble their corresponding Franck Condon structures. Also interesting, very similar vertical emission energies have been calculated for the monomer (3.30 eV) and the dimer (3.25 eV), consistently with the weak interaction between the two monomers. Finally, for the sake of deciphering the origin of the solvent-dependent emission spectra, which is clearly not purely electronic, we have modelled the vibrationally-resolved version of the emission spectra of the monomer and dimer (see bottom panel of Figure 6). Despite the limited resolution of the vibronic bands, which may be ascribable to the level of theory used in the calculation of the normal modes (see Supporting Information for further details), the calculated spectra show interesting features which can help to provide some insight into the experimentally reported changes. In particular, upon aggregation the high energy region of the emission band of the monomer experiences a decrease in intensity. Concomitant to that, a significant increase of the intensity of the absorption signal for wavelengths longer than 525 nm is observed, that would readily explain the green color adopted by the solution upon increasing the water fraction of the solvent and would nicely mimic the smoother decay of the red tail of the emission band of the experimental spectrum.

Conclusion

The benchtop bottom-up synthesis of a 3D molecular nanographene has been described. Tetrahedraphene **1** is formed by four HBC units linked to a central sp^3 carbon, leading to a tetrahedral arrangement of the HBCs. The facile preparation of **1** consists only in three synthetic steps (Sonogashira cross-coupling, [4+2] cycloaddition and Scholl oxidation). Tetrahedraphene **1** has been fully characterized by HR-MS, FT-IR and NMR. X-ray diffraction experiment shows a structure with high symmetry, only one fourth of the molecule is present in the asymmetric unit and the central carbon is located at an inversion center from a fourfold rotoinversion axis.

The electrochemical properties of tetrahedraphene **1** slightly differ when comparing with ^{t}Bu-HBC. While the first reduction potential remains practically unchanged ($E^1_{1/2\ red} = -2.45$ V for **1** and $E^1_{1/2\ red} = -2.46$ V for ^{t}Bu-HBC), **1** shows two very close oxidation potentials ($E^1_{1/2\ ox} = 0.67$ V and $E^2_{1/2\ ox} = 0.80$ V) instead of one oxidation potential of ^{t}Bu-HBC ($E^1_{1/2\ ox} = 0.63$ V). This may be due to a repulsive interaction between the two positive charges with the second oxidation. The electrochemical band gap of **1** and ^{t}Bu-HBC, calculated from the onset first reduction and the onset first oxidation potentials also remains unchanged (2.85 eV for **1** and 2.82 eV for ^{t}Bu-HBC). These values are in good agreement with the computationally predicted HOMO–LUMO gap of 3.49 eV.

The fluorescence properties of tetrahedraphene **1** were evaluated both in solution and in the solid state. In $CHCl_3$ solution, **1** shows blue fluorescence, similar to that shown by ^{t}Bu-HBC, with maxima at 467, 477, 487, 496, 521, 531, 542 nm. However, **1** undergoes an increase in fluorescence intensity when adding a water volume fraction of up to 30 % in a process of aggregation-induced emission enhancement (AIEE). With water volume above 50 % and in the precipitated solid, the fluorescence color changes to yellow with maxima at 543 and 582 nm in an aggregation-induced emission (AIE) process. These changes in fluorescence could be attributed to both the restriction of the rotational and vibrational motions of the four HBCs of **1** avoiding the non-radiative relaxation of the excited state, and to a change

in the emission profile of the aggregated species, which shifts the emission maximum to longer wavelengths.

AIE is an emerging concept in luminescence with a great potential in a variety of fields including chemistry, biology, materials science, and biomedical applications.[25] In this regard, to the best of our knowledge, AIE in molecular nanographenes has not been properly addressed so far, and only a few related cases involving N-containing NGs have been described in the literature.[22] Therefore, we feel that the results here reported based on an all-carbon compound pave the way to the search for new luminogenic NGs by design exhibiting amazing AIE properties.

Acknowledgements

A. O., J. M. F.-G. and N.M. acknowledge financial support from the Spanish MICIN (Project PID2020-114653RB–I00), they also acknowledge financial support from the ERC (SyG TOMATTO ERC-2020-951224) and from the "-(MAD2D-CM)-UCM" project funded by Comunidad de Madrid, by the Recovery, Transformation and Resilience Plan, and by NextGenera-tionEU from the European Union. I.C. and F.R.-G. also thankfully acknowledge financial support from the PID2021-125207NB-C31 project of the Ministerio de Ciencia e Innovación of Spain **and the generous allocation of computer time and continued technical support by the Centro de Computación Científica of the UAM (CCC-UAM).**

Conflict of Interest

The authors declare no conflict of interest.

Data Availability Statement

Research data are not shared.

Keywords: 3D Nanographene · Aggregation-Induced Emission · Bottom-up Synthesis · Molecular Nanographene · X-Ray Diffraction

[1] a) M. Dvorak, W. Oswald, Z. G. Wu, *Sci. Rep.* **2013**, *3*, 2289; b) J. Z. Liu, B. W. Li, Y. Z. Tan, A. Giannakopoulos, C. Sánchez-Sánchez, D. Beljonne, P. Ruffieux, R. Fasel, X. L. Feng, K. Müllen, *J. Am. Chem. Soc.* **2015**, *137*, 6097; c) V. G. Desyatkin, W. B. Martin, A. E. Aliev, N. E. Chapman, A. F. Fonseca, D. S. Galvão, E. R. Miller, K. H. Stone, Z. Wang, D. Zakhidov, F. T. Limpoco, S. R. Almahdali, S. M. Parker, R. H. Baughman, V. O. Rodionov, *J. Am. Chem. Soc.* **2022**, *144*, 17999.

[2] a) Z. Sun, Q. Ye, C. Chi, J. Wu, *Chem. Soc. Rev.* **2012**, *41*, 7857; b) Z. Wang, R. Li, Y. Chen, Y.-Z. Tan, Z. Tu, X. J. Gao, H. Dong, Y. Yi, Y. Zhang, W. Hu, K. Müllen, L. Chen, *J. Mater. Chem. C* **2017**, *5*, 1308; c) Z. Chen, A. Narita, K Müllen, *Adv. Mater.* **2020**, *32*, 2001893.

[3] a) A. A. Peyghan, J. Beheshtian, *Thin Solid Films* **2020**, *704*, 137979; b) G. Wang, M. Yu, X. Feng, *Chem. Soc. Rev.* **2021**, *50*, 2388.

[4] a) P. Namdari, B. Negahdari, A. Eatemadi, *Biomed. Pharmacother.* **2017**, *87*, 209; b) N. Panwar, A. M. Soehartono, K. K. Chan, S. Zeng, G. Xu, J. Qu, P. Coquet, K. T. Yong, X. Chen, *Chem. Rev.* **2019**, *119*, 9559; c) Y. R. Kumar, K. Deshmukh, K. K. Sadasivuni, S. K. K. Pasha, *RSC Adv.* **2020**, *10*, 23861.

[5] a) Z. Wang, Q. Jingjing, X. Wang, Z. Zhang, Y. Chen, X. Huang, W. Huang, *Chem. Soc. Rev.* **2018**, *47*, 6128; b) E. Fresta, J. Dosso, J. Cabanillas-González, D. Bonifazi, R. D. Costa, *ACS Appl. Mater. Interfaces* **2020**, *12*, 28426; c) S. Gao, Z. Cui, F. Li, *Chem. Soc. Rev.* **2023**, *52*, 2875.

[6] a) J. Shen, Y. Zhu, X. Yang, C. Li, *Chem. Commun.* **2012**, *48*, 3686; b) N. Martín, *Adv. Energy Mater.* **2017**, *7*, 1601102; c) S. Das, D. Pandey, J. Thomas, T. Roy, *Adv. Mater.* **2019**, *31*, 1802722.

[7] a) X. Li, M. Rui, J. Song, Z. Shen, H. Zeng, *Adv. Funct. Mater.* **2015**, *25*, 4929; b) J. M. Tour, *Chem. Mater.* **2014**, *26*, 163; c) M. Vázquez-Nakagawa, L. Rodríguez-Pérez, M. A. Herranz, N. Martín, *Chem. Commun.* **2016**, *52*, 665; d) Y. Yan, J. Gong, J. Chen, Z. Zeng, W. Huang, K. Pu, J. Liu, P. Chen, *Adv. Mater.* **2019**, *31*, e1808283; e) M. Vázquez-Nakagawa, L. Rodríguez-Pérez, N. Martín, M. A. Herranz, *Angew. Chem. Int. Ed.* **2022**, *61*, e202211365.

[8] a) C. D. Simpson, G. Mattersteig, K. Martin, L. Gherghel, R. E. Bauer, H. J. Räder, K. Müllen, *J. Am. Chem. Soc.* **2004**, *126*, 3139; b) T. Nishiuchi, X. Feng, V. Enkelmann, M. Wagner, K. Müllen, *Chem. Eur. J.* **2012**, *18*, 16621; c) X. Y. Wang, J. I. Urgel, G. B. Barin, K. Eimre, M. Di Giovannantonio, A. Milani, M. Tommasini, C. A. Pignedoli, P. Ruffieux, X. Feng, R. Fasel, K. Müllen, A. Narita, *J. Am. Chem. Soc.* **2018**, *140*, 9104; d) A. Jolly, D. Miao, M. Daigle, J. F. Morin, *Angew. Chem. Int. Ed.* **2020**, *59*, 4624.

[9] a) J. Holzwarth, K. Y. Amsharov, D. I. Sharapa, D. Reger, K. Roshchyna, D. Lungerich, N. Jux, F. Hauke, T. Clark, A. Hirsch, *Angew. Chem. Int. Ed.* **2017**, *56*, 12184; b) P. Izquierdo-García, J. M. Fernández-García, J. Perles, I. Fernández, N. Martín, *Angew. Chem. Int. Ed.* **2023**, *62*, e202215655.

[10] a) M. Grzybowski, K. Skonieczny, H. Butenschön, D. T. Gryko, *Angew. Chem. Int. Ed.* **2013**, *52*, 9900; b) Z. Liu, S. Fu, X. Liu, A. Narita, P. Samorì, M. Bonn, H. I. Wang, *Adv. Sci.* **2022**, *9*, 2106055; c) Y. Zhang, S. H. Pun, Q. Miao, *Chem. Rev.* **2022**, *122*, 14554.

[11] a) S. H. Pun, Q. Miao, *Acc. Chem. Res.* **2018**, *51*, 1630; b) J. M. Fernández-García, P. J. Evans, S. Medina Rivero, I. Fernández, D. García-Fresnadillo, J. Perles, J. Casado, N. Martín, *J. Am. Chem. Soc.* **2018**, *140*, 17188; c) M. A. Majewski, M. Stępień, *Angew. Chem. Int. Ed.* **2019**, *58*, 86; d) G. Báti, D. Csókas, T. Yong, S. M. Tam, R. R. S. Shi, R. D. Webster, I. Pápai, F. García, M. C. Stuparu, *Angew. Chem. Int. Ed.* **2020**, *59*, 21620; e) Chaolumen, I. A. Stepek, K. E. Yamada, H. Ito, K. Itami, *Angew. Chem. Int. Ed.* **2021**, *60*, 23508; f) S. Zank, J. M. Fernández-García, A. J. Stasyuk, A. A. Voityuk, M. Krug, M. Solà, D. M. Guldi, N. Martín, *Angew. Chem. Int. Ed.* **2022**, *61*, e202112834; g) Z. Zhou, Y. Zhu, J. M. Fernández-García, Z. Wei, I. Fernández, M. A. Petrukhina, N. Martín, *Chem. Commun.* **2022**, *58*, 5574; h) S. Ramírez-Barroso, F. Romeo-Gella, J. M. Fernández-García, S. Feng, L. Martínez-Fernández, D. García-Fresnadillo, I. Corral, N. Martín, R. Wannemacher, *Adv. Mater.* **2023**, *35*, e2212064.

[12] a) C. M. Cruz, S. Castro-Fernández, E. Maçôas, J. M. Cuerva, A. G. Campaña, *Angew. Chem. Int. Ed.* **2018**, *57*, 14782; b) C. M. Cruz, I. R. Márquez, S. Castro-Fernández, J. M. Cuerva, E. Maçôas, A. G. Campaña, *Angew. Chem. Int. Ed.* **2019**, *58*, 8068; c) J. Ma, Y. Fu, E. Dmitrieva, F. Liu, H. Komber, F. Hennersdorf, A. A. Popov, J. J. Weigand, J. Liu,

X. Feng, *Angew. Chem. Int. Ed.* **2020**, *59*, 5637; d) D. Reger, P. Haines, K. Y. Amsharov, J. A. Schmidt, T. Ullrich, S. Bönisch, F. Hampel, A. Görling, J. Nelson, K. E. Jelfs, D. M. Guldi, N. Jux, *Angew. Chem. Int. Ed.* **2021**, *60*, 18073; e) P. Izquierdo-García, J. M. Fernández-García, I. Fernández, J. Perles, N. Martín, *J. Am. Chem. Soc.* **2021**, *143*, 11864; f) Z. Zhou, J. M. Fernández-García, Y. Zhu, P. J. Evans, R. Rodríguez, J. Crassous, Z. Wei, I. Fernández, M. A. Petrukhina, N. Martín, *Angew. Chem. Int. Ed.* **2022**, *61*, e202115747; g) P. Izquierdo-García, J. M. Fernández-García, S. Medina Rivero, M. Samal, J. Rybacek, L. Bednarova, S. Ramírez-Barroso, F. J. Ramírez, R. Rodríguez, J. Perles, D. García-Fresnadillo, J. Crassous, J. Casado, I. G. Starà, N. Martín, *J. Am. Chem. Soc.* **2023**, *145*, 11599; h) Y. Zhu, J. Wang, *Acc. Chem. Res.* **2023**, *56*, 363.

[13] a) K. Y. Cheung, C. K. Chan, Z. Liu, Q. Miao, *Angew. Chem. Int. Ed.* **2017**, *56*, 9003; b) A. Bedi, O. Gidron, *Acc. Chem. Res.* **2019**, *52*, 2482; c) S. Castro-Fernández, C. M. Cruz, I. F. A. Mariz, I. R. Márquez, V. G. Jiménez, L. Palomino-Ruiz, J. M. Cuerva, E. Maçôas, A. G. Campaña, *Angew. Chem. Int. Ed.* **2020**, *59*, 7139; d) J. Urieta-Mora, M. Krug, W. Alex, J. Perles, I. Fernández, A. Molina-Ontoria, D. M. Guldi, N. Martín, *J. Am. Chem. Soc.* **2020**, *142*, 4162; e) Y. Gao, X. Hua, W. Jiang, C. L. Sun, C. Yuan, Z. Liu, H. L. Zhang, X. Shao, *Angew. Chem. Int. Ed.* **2022**, *61*, e202210924.

[14] a) J. M. Fernández-García, P. J. Evans, S. Filippone, M. A. Herranz, N. Martín, *Acc. Chem. Res.* **2019**, *52*, 1565; b) J. M. Fernández-García, P. Izquierdo-García, M. Buendía, S. Filippone, N. Martín, *Chem. Commun.* **2022**, *58*, 2634; c) H. V. Anderson, N. D. Gois, W. A. Chalifoux, *Org. Chem. Front.* **2023**, *10*, 4167; d) R. Li, D. Wang, S. Li, P. An, *Beilstein J. Org. Chem.* **2023**, *19*, 736.

[15] P. T. Herwig, V. Enkelmann, O. Schmelz, K. Müllen, *Chem. Eur. J.* **2000**, *6*, 1834.

[16] J. N. Smith, J. M. Hook, N. T. Lucas, *J. Am. Chem. Soc.* **2018**, *140*, 1131.

[17] H. J. Yen, H. Tsai, M. Zhou, E. F. Holby, S. Choudhury, A. Chen, L. Adamska, S. Tretiak, T. Sánchez, S. Iyer, H. Zhang, L. Zhu, H. Lin, L. Dai, G. Wu, H. L. Wang, *Adv. Mater.* **2016**, *28*, 10250.

[18] a) B. Alameddine, O. F. Aebischer, B. Heinrich, D. Guillon, B. Donnio, T. A. Jenny, *Supramol. Chem.* **2014**, *26*, 125; b) B. Alameddine, R. S. Anju, S. Shetty, N. Baig, F. Al-Sagheer, S. Al-Mousawi, A. T. Jenny, *New J. Chem.* **2017**, *41*, 6025.

[19] a) J. Mei, Y. Hong, J. W. Y. Lam, A. Qin, Y. Tang, B. Z. Tang, *Adv. Mater.* **2014**, *26*, 5429; b) N. L. C. Leung, N. Xie, W. Yuan, Y. Liu, Q. Wu, Q. Peng, Q. Miao, J. W. Y. Lam, B. Z. Tang, *Chem. Eur. J.* **2014**, *20*, 15349.

[20] a) M. Gao, B. Z. Tang, *ACS Sens.* **2017**, *2*, 1382; b) Z. He, C. Ke, B. Z. Tang, *ACS Omega* **2018**, *3*, 3267; c) C. Shen, F. Gan, G. Zhang, Y. Ding, J. Wang, R. Wang, J. Crassous, H. Qiu, *Mater. Chem. Front.* **2020**, *4*, 837; d) B. Liu, B. Z. Tang, *Angew. Chem. Int. Ed.* **2020**, *59*, 9788; e) N. Baig, S. Shetty, R. Tiwari, S. K. Pramanik, B. Alameddine, *ACS Omega* **2022**, *7*, 45732.

[21] a) Z. Zhao, B. He, B. Z. Tang, *Chem. Sci.* **2015**, *6*, 5347; b) R. Furue, T. Nishimoto, I. S. Park, J. Lee, T. Yasuda, *Angew. Chem. Int. Ed.* **2016**, *55*, 7171; c) Z. Zhao, H. Zhang, J. W. Y. Lam, B. Z. Tang, *Angew. Chem. Int. Ed.* **2020**, *59*, 9888.

[22] H. Luo, J. Liu, *Angew. Chem. Int. Ed.* **2023**, *62*, e202302761.

[23] B. A. G. Hammer, K. Müllen, *Chem. Rev.* **2016**, *116*, 2103.

[24] Deposition number 2281440 (for **1**) contains the supplementary crystallographic data for this paper. These data are provided free of charge by the joint Cambridge Crystallographic Data Centre and Fachinformationszentrum Karlsruhe Access Structures service.

[25] For a recent review, see: H. Wang, Q. Li, P. Alam, H. Bai, V. Bhalla, M. R. Bryce, M. Cao, C. Chen, S. Chen, X. Chen, Y. Chen, Z. Chen, D. Dang, D. Ding, S. Ding, Y. Duo, M. Gao, W. He, X. He, X. Hong, Y. Hong, J.-J. Hu, R. Hu, X. Huang, T. D. James, X. Jiang, G. Konishi, R. T. K. Kwok, J. W. Y. Lam, C. Li, H. Li, K. Li, N. Li, W.-J. Li, Y. Li, X.-J. Liang, Y. Liang, B. Liu, G. Liu, X. Liu, X. Lou, X.-Y. Lou, L. Luo, P. R. McGonigal, Z.-W. Mao, G. Niu, T. C. Owyong, A. Pucci, J. Qian, A. Qin, Z. Qiu, A. L. Rogach, B. Situ, K. Tanaka, Y. Tang, B. Wang, D. Wang, J. Wang, W. Wang, W.-X. Wang, W.-J. Wang, X. Wang, Y.-F. Wang, S. Wu, Y. Wu, Y. Xiong, R. Xu, C. Yan, S. Yan, H.-B. Yang, L.-L. Yang, M. Yang, Y.-W. Yang, J. Yoon, S.-Q. Zang, J. Zhang, P. Zhang, T. Zhang, X. Zhang, X. Zhang, N. Zhao, Z. Zhao, J. Zheng, L. Zheng, Z. Zheng, M.-Q. Zhu, W.-H. Zhu, H. Zou, B. Z. Tang, *ACS Nano* **2023**, *17*, 14347.

Manuscript received: August 22, 2023
Accepted manuscript online: October 17, 2023
Version of record online: October 31, 2023